Ferromagnetism and metal-insulator transition in F-doped LaMnO₃

Ekta Yadav [1,*] Pramod Ghising [1,*,†] K. P. Rajeev,[1] and Z. Hossain[1,2,‡]

[1]*Department of Physics, Indian Institute of Technology, Kanpur 208016, India*
[2]*Institute of Low Temperature and Structure Research, Polish Academy of Sciences, Okólna 2, 50-422 Wrocław, Poland*

We present our studies on polycrystalline samples of fluorine doped LaMnO₃ (LaMnO$_{3-y}$F$_y$). LaMnO$_{3-y}$F$_y$ exhibits remarkable magnetic and electrical properties. It shows ferromagnetic and metallic behavior with a high Curie temperature of $\approx$239 K and a high magnetoresistance of -64%. This drastic change in magnetic properties in comparison to pure LaMnO₃ is ascribed to the presence of mixed-valence Mn ions driven by the F-doping at the O-sites, which enables double exchange in LaMnO$_{3-y}$F$_y$. Furthermore, the resistivity data exhibits two peaks at 239 and 213 K, respectively. Our results point towards the possibility of multiple double exchange hopping paths of two distinct resistances existing simultaneously in the sample below 213 K.

I. INTRODUCTION

Perovskite manganites have been known to exhibit exotic phenomena such as colossal magnetoresistance (CMR), ferromagnetism, half-metallic behavior [1–3], etc. Perovskites have the chemical formula ABO₃. In perovskite manganites the smaller B ions (transition metals) sit at the center of an oxygen octahedra BO₆, as shown in Fig. 1. The exotic properties of manganites are derived from the parent compound LaMnO₃ (LMO), which is an insulating A-type antiferromagnet with a Néel temperature of 140 K [4–6]. LMO being an antiferromagnetic insulator, is "interesting but useless," to quote Louis Néel from his Nobel prize speech. A common strategy to extract "useful" properties out of LMO is doping the A-sites with divalent atoms. A large number of these exciting phenomena results from doping the La-site of the parent compound LaMnO₃. Prominent examples include compounds such as La$_{1-x}$Sr$_x$MnO₃ (LSMO), La$_{1-x}$Pr$_x$Ca$_{0.375}$MnO₃ (LPCMO), La$_{1-x}$Ca$_x$MnO₃ (LCMO) etc., which exhibit rich phase diagrams at various dopant concentrations [7–11]. It is observed that for a certain range of the value of the doping concentration x, we can induce ferromagnetism and metallic properties in LMO. In the case of LSMO, the range of x is $0.2 < x < 0.5$ [12,13].

Doping at the A-site or the La-site with divalent ions results in a mixed valency of the Mn ions, i.e., both Mn^{3+} and Mn^{4+} [14,15]. The Mn^{3+} and Mn^{4+} ions occupy the B-site of the LMO lattice. Mixed valency of Mn is essential for the ferromagnetic and metallic behavior, which result from the double exchange (DE) hopping of electrons along the Mn^{3+}-O-Mn^{4+} chains from one B site to another B site in the manganite lattice [16]. The DE hopping depends on the Mn^{3+}-O-Mn^{4+}

bond angle θ [17]. Double exchange hopping is maximum for $\theta_{\circ} = 180°$, and decreases as θ deviates from $\theta_{\circ}$. Consequently, ferromagnetic and metallic properties of manganites are very sensitive to distortions of the MnO₆ octahedra.

An alternate route to tune the properties of manganites is doping at the anion sites. Although La site doping of LMO has been studied extensively, there are very few reports on O-site doping of LMO. One possible way is to dope the O-site with fluorine [18,19]. Here, we present our studies on F doping of LMO sample. We observe, that on F doping, the LMO sample exhibits ferromagnetic and metallic behavior with high values of magnetoresistance (MR). The ferromagnetic properties are at par with La-site doped manganites.

II. EXPERIMENTAL DETAILS

LaMnO$_{3-y}$F$_y$ (LMOF) samples (with $y = 0.25, 0.50, 0.75$) were synthesized by the solid-state reaction method. The pure sample LaMnO₃ is represented as LMO and the F-doped samples are represented as LMOF-S1/S2/S3 for $y = 0.25, 0.50, 0.75$ respectively. Powders of La₂O₃, Mn₂O₃ and LaF₃ were taken in stoichiometric ratios and were ground and mixed thoroughly using a mortar and pestle for 45 minutes. The ground powder was sintered in air for 24 hours at a fixed temperature of 600, 700, 800, 900, 1000, and 1100 °C. Before each sintering process, the powder was thoroughly reground. Finally, the sintered powder was pressed into a pellet and annealed in air at 900 °C.

X-ray diffraction (XRD) and energy-dispersive x-ray spectroscopy (EDX) was used for structural characterization and elemental analysis of the samples, respectively. XRD was performed using a Panalytical Expert Pro x-ray diffractometer with a Cu-$K_{\alpha 1}$ radiation. JXA-8230 Electron Probe Microanalyzer (JEOL Ltd.) was used for determining the chemical composition. Iodometric titration was also used for determination of oxygen content. The electrical and magnetotransport measurements were carried out in a Quantum design physical property measurement system (PPMS). Standard four-probe technique was used for the electrical resistivity measurements.

---

*These authors contributed equally to this work.

†Present address: Center for Integrated Nanostructure Physics (CINAP), Institute for Basic Science (IBS), Sungkyunkwan University, Suwon 16419, Republic of Korea.
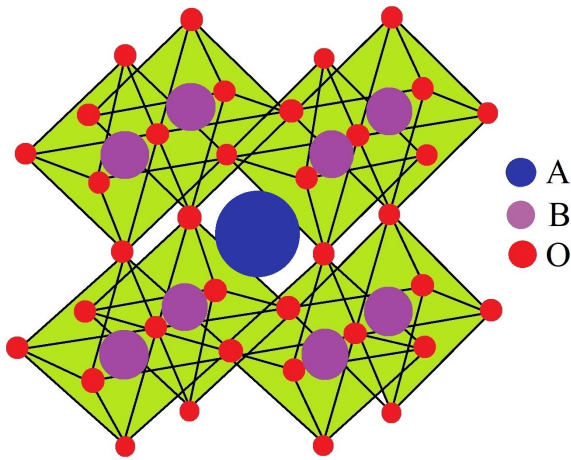
‡zakir@iitk.ac.in

FIG. 1. Structure of a perovskite oxide with the chemical formula ABO_3. The B ion sits at the center of an oxygen octahedra BO_6.

X-ray photoemission spectroscopy (XPS) measurement (using Al-K_α x-ray source, $h\nu = 1486.6$ eV, PHI 5000 Versa Probe II, FEI Inc.) was carried out to determine the valence states of Mn and La in LMOF.

III. RESULT AND DISCUSSION

The results of the XRD measurement carried out on the $LaMnO_{3-y}F_y$ sample with intended F-doping value of $y = 0.5$ is shown in Fig. 2. XRD result of a LMO control sample is also shown in Fig. 2 (red line) for comparison. The XRD data reveal coinciding LMO and LMOF-S2 peaks, indicating that LMOF-S2 also maintains the same perovskite structure as LMO. The absence of extra peaks in the XRD data confirms the absence of any secondary phases in the LMOF-S2 sample. The lattice parameters of LMO sample was determined to be $a = 0.5483$ nm, $b = 0.7803$ nm, $c = 0.5543$ nm which are comparable to the values reported by others [20]. The lattice parameters of LMOF-S2 are $a = 0.5477$ nm, $b = 0.7802$ nm, $c = 0.5542$ nm. The grain size of the different
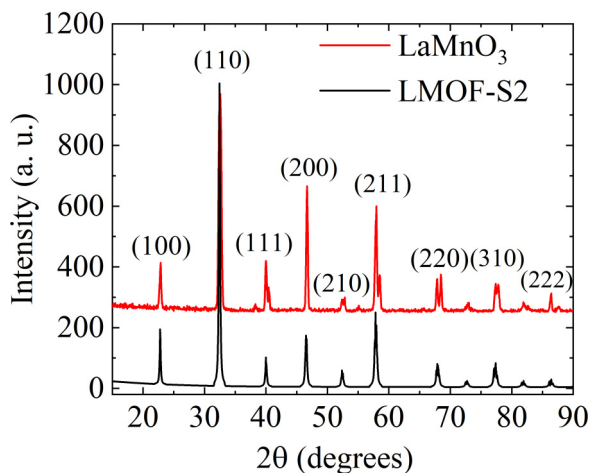

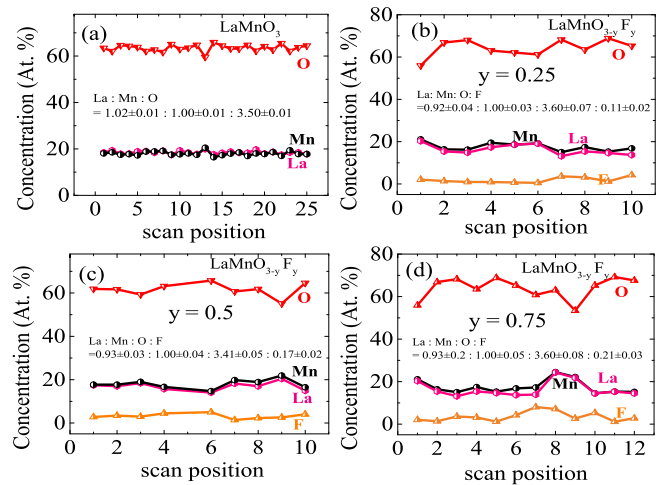FIG. 2. Powder x-ray diffraction result of $LaMnO_3$ and LMOF-S2.

FIG. 3. EDX average area points scan of various LMO samples: (a) undoped, (b) LMOF-S1, (c) LMOF-S2, (d) LMOF-S3.

LMOF samples determined using Scherrer's formula are 29, 39, and 32 nm for different F concentrations with $y = 0.25$, $y = 0.50$, and $y = 0.75$, respectively. EDX measurements (at room temperature) on different regions of the LMOF sample show La deficiency. EDX data for undoped and F-doped LMO samples are shown in Fig. 3 along with atomic ratio of all elements. For undoped LMO, EDX [Fig. 3(a)] reveals La : Mn : O $= 1.02 \pm 0.01 : 1.00 \pm 0.01 : 3.50 \pm 0.01$ with excess oxygen and with atomic concentration ($\pm$ standard error) La $= 18.48 \pm 0.46$, Mn $= 18.04 \pm 0.78$, O $= 63.44 \pm 1.99$. The atomic ratio averaged over many point scans for different F-doped samples are depicted in the Figs. 3(b)–3(d). For $y = 0.5$ F-doped LMO it is La : Mn : O : F $= 0.93 \pm 0.03 : 1 \pm 0.04 : 3.41 \pm 0.05 : 0.17 \pm 0.02$ (with at. concentration La $= 17.00 \pm 0.60$, Mn $= 18.10 \pm 0.65$, F $= 3.21 \pm 0.35$, O $= 61.54 \pm 0.97$). For undoped LMO, at% of the cations are La $= 18.48$ and Mn $= 18.04$. Similarly, for F-doped LMO it is La $= 17.00$ and Mn $= 18.10$. It is clearly seen that the Mn content is more or less the same in both the doped and undoped LMO, whereas La content decreases in the F-doped sample. Thus, it is reasonable to normalize with respect to Mn rather than La. For all F-doped samples, fluorine concentration is seen to increase monotonically (0.11 ± 0.02, 0.17 ± 0.02, 0.21 ± 0.03) but is less than the intended value of $y = 0.25$, 0.5 and 0.75, respectively. EDX data show considerably higher value of oxygen concentration for both undoped and F-doped LMO.

The low atomic number of oxygen makes it difficult for EDX measurements to make reliable estimate of its concentration in oxides. Therefore, we also performed iodometric titration [21,22] to further determine the oxygen concentration in both doped and undoped LMO samples. Titration involves slowly adding a chemical substance to a reaction mixture until the chemical change is complete. For undoped LMO, iodometric titration yields a concentration of 3.21 with an excess oxygen of 0.21. The excess oxygen obtained with this method is much less than the EDX value of 0.5 for undoped LMO. Similarly, for $y = 0.5$ F-doped LMO, it shows a concentration of 3.15, with excess oxygen of 0.15. This is again less than the

TABLE I. EDX estimated values for all F-doped samples.

Sample name	y	Intended composition	EDX measured composition
LMO	0	$LaMnO_3$	$La_{1.02}Mn_{1.00}O_{3.50}$
LMOF-S1	0.25	$LaMnO_{2.75}F_{0.25}$	$La_{0.92}Mn_{1.00}O_{3.60}F_{0.11}$
LMOF-S2	0.50	$LaMnO_{2.50}F_{0.50}$	$La_{0.93}Mn_{1.00}O_{3.40}F_{0.17}$
LMOF-S3	0.75	$LaMnO_{2.25}F_{0.75}$	$La_{0.93}Mn_{1.00}O_{3.60}F_{0.21}$

excess oxygen value obtained from EDX for $y = 0.5$ F-doped LMO (which is 0.41). Combining the EDX and iodometric titration we conclude that the undoped and doped samples have some excess oxygen and there is a systematic increase of F-content for different F-doped samples. The excess oxygen is due to sintering and annealing of the samples in air. The intended compositions and EDX determined compositions of the pure and F-doped samples are presented in a tabular form in Table I.

A very interesting feature of our LMOF-S2 sample is the observation of a ferromagnetic transition close to room temperature. Figure 4(a) displays the results of the field cooled (FC) and zero-field cooled (ZFC) magnetization measurement as a function of temperature. For the FC measurement the sample was cooled in an applied field of 2000 Oe and the data acquisition was carried out during the heating cycle. The Curie temperature T_{C1} of the ferromagnetic transition is 238 K. Another ferromagnetic transition is also observed in the $M(T)$ data at $T_{C2} = 217$ K, indicating the presence of two distinct ferromagnetic exchanges in the LMOF sample. $M(H)$ measurement done at 120 K [shown in Fig. 4(b)] exhibits a hysteresis loop typical of ferromagnets, further confirming the ferromagnetic nature of LMOF-S2 below the Curie temperature.

To further probe the nature of ferromagnetism we carried out electrical transport measurements on the LMOF-S2 sample, the results of which are shown in Fig. 5(a). The sample exhibits a metallic behavior with a metal-insulator transition (MIT) at $T_{p1} = 239$ K and another slightly broad resistivity peak at $T_{p2} = 213$ K. It is to be noted that the undoped LMO control sample exhibits an insulating behavior without any MIT as can be seen in the upper inset of Fig. 5(a). Hall measurement carried out at 300 K on the LMOF-S2 sample reveals hole-type carriers, inferred from the positive slope of the ρ_{xy}-H curve [shown in lower inset of Fig. 5(a)]. The carrier concentration was determined to be 0.18×10^{22} cm^{-3}. For comparison, we also carried out resistivity measurements on two additional samples LMOF-S1 and LMOF-S3. Their resistivity data also exhibit metallic behavior with similar double peaks as shown in Fig. 5(b). The field dependent resistivity data of LMOF is shown in Fig. 6(a). In the presence of a 7 T magnetic field both the resistivity peaks at T_{p1} and T_{p2} are suppressed and are also shifted to higher temperatures by 40 and 22 K, respectively, suggestive of a similar magnetic origin of the two peaks. Moreover, a large magnetoresistance [MR = $[\rho(H) - \rho(0)]/\rho(0)$] of about -64% and -50% is also observed at T_{p1} and T_{p2}, respectively. The MR below T_{p2} show no significant change with temperature. Interestingly, the onset of the ferromagnetic transition T_{C1} and the MIT
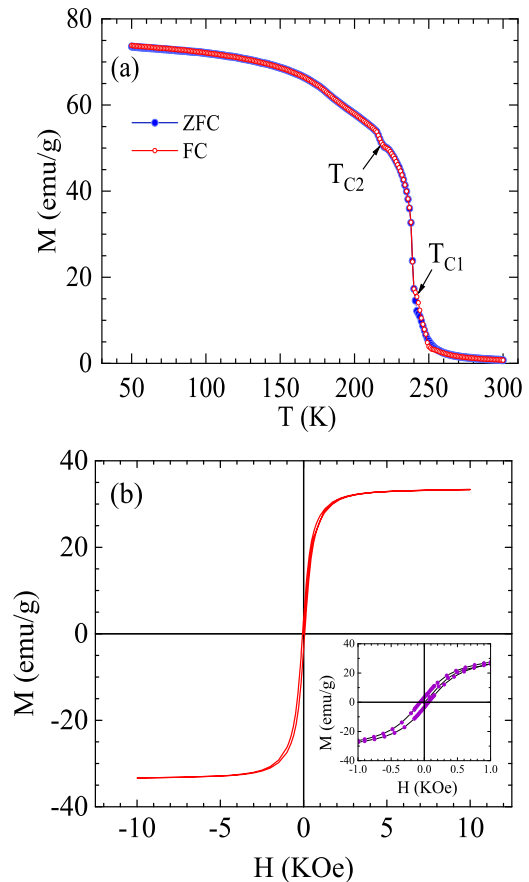

FIG. 4. (a) Results of FC and ZFC-$M(T)$ measurements carried out on LMOF-S2. Two magnetic transitions in the $M(T)$ data are apparent at $T_{C1} = 238$ K and $T_{C2} = 217$ K. (b) $M(H)$ measurement of the LMOF-S2 sample at 120 K ($<T_{C1}, T_{C2}$) exhibits a hysteresis loop, which confirms the ferromagnetic nature of LMOF-S2. The inset shows the blown up view of the central region of the hysteresis loop. The coercivity is 64 Oe.

temperature T_{p1} coincide [shown in Fig. 6(b)]. This result strongly suggests that the ferromagnetic and the metallic properties of LMOF-S2 are related. One such example of concurrent ferromagnetic and metallic behavior in A-site doped LMO (such as LSMO, LCMO) results from double exchange mechanism [13,23], where the charge carriers are holes. Such DE mechanism in LMOF-S2 is only possible in the presence of the mixed valence of Mn. Also, the resistivity peak T_{p2} coincides with the ferromagnetic transition in the $M(T)$ data at $T_{C2} = 217$ K, which further indicates that T_{p2} is related to ferromagnetic properties of the sample.

The core-level XPS spectra of the LMOF-S2 sample is shown in Fig. 7. Mn in LMOF-S2 exhibits a mixed-valence state as is apparent from its XPS spectra displayed in Fig. 7(a). Analysis of the XPS spectra for Mn reveals a valence state of Mn^{2+}, Mn^{3+}, and Mn^{4+}. The Mn^{2+}, Mn^{3+}, and Mn^{4+} peak positions occur at 641.0, 642.1, 643.6 and 653.0, 653.6, 654.6 for the $2p_{3/2}$ and $2p_{1/2}$ spin-orbit split peaks, respectively, which are similar to earlier reported values [24,25]. The XPS spectra of La [shown in Fig. 7(b)] determines its valence state to be La^{3+} [26]. The deconvoluted La $3d_{5/2}$ and $3d_{3/2}$ show
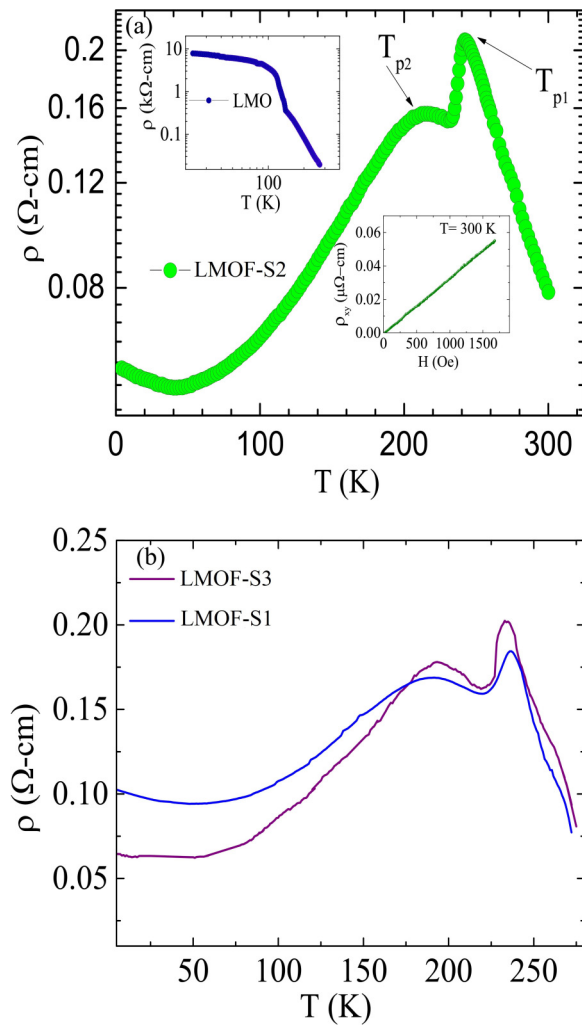
FIG. 5. (a) Electrical resistivity of LMOF-S2 exhibits metallic behavior with two distinct resistivity peaks at $T_{p1} = 239$ K and $T_{p2} = 213$ K. On the other hand, pure LMO sample exhibits insulating behavior as is observed from its resistivity data shown in the upper inset. The bottom inset shows the Hall measurement on the LMOF-S2 sample at 300 K. The positive slope in the Hall measurement indicates hole-type carriers in LMOF-S2. (b) Resistivity measurement on samples with different F concentrations (LMOF-S1 and LMOF-S3) also exhibit metallic behavior with similar double peaks.

FIG. 6. (a) Magnetic-field-dependent resistivity of the LMOF-S2 sample. At T_{p1} and T_{p2} a large magnetoresistance of -64% and -50% is observed. MR (shown on the right axis) is independent of temperature below T_{p2}. (b) Comparison of the resistivity peaks with the magnetic transition temperature of LMOF-S2. It is observed that the two magnetic transition temperatures in $M(T)$ correspond to the two resistivity peaks in $\rho(T)$.

multiple peaks due to La binding with oxide and hydroxyl species and also final-state effects. The peaks A, C, E, and G correspond to La binding with oxygen while the peaks B, D, and F correspond to La binding with hydroxyl species [26]. F 1s and O 1s XPS spectra are shown in Figs. 7(c) and 7(d), respectively. The additional peak at 531.5 eV in the O 1s XPS spectra is ascribed to the formation of hydroxyl species [27].

Thus, F doping induces a mixed-valence state of the Mn ions. Using resonant inelastic x-ray spectroscopy, Orgiani *et al.* established that Mn^{2+} ions occupy the La site in LMO [28], which probably explains the La deficiency in our LMOF sample. The origin of the Mn^{2+} is due to the sample's tendency to maintain charge neutrality upon F doping. Mn^{2+} ions occupying the La-sites is analogous to A-site doping of
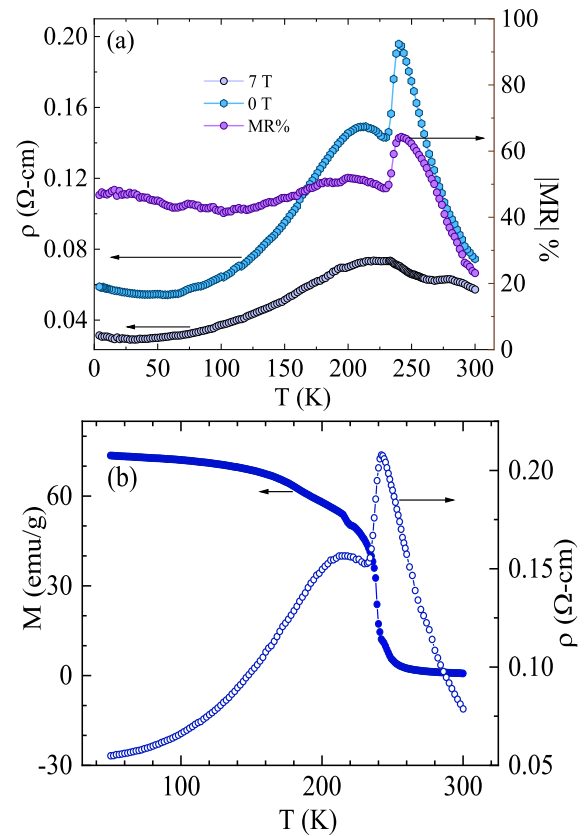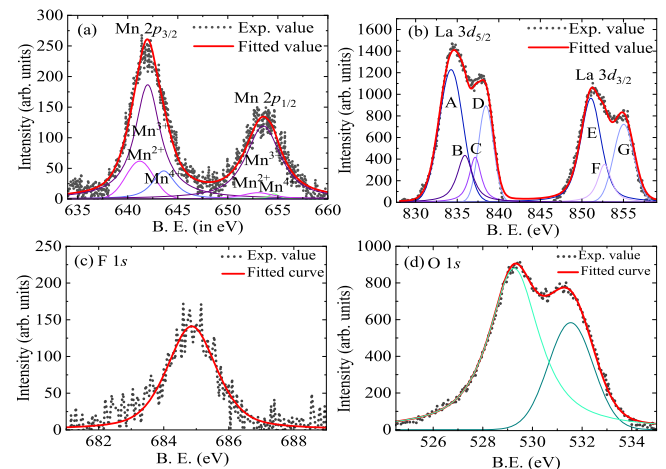

FIG. 7. XPS spectrum of LMOF-S2. The XPS data were fit using a combination of Gaussian-Lorentzian peak shapes. (a) Mn 2p spectrum with its two spin-orbit doublet. The presence of Mn^{2+}, Mn^{3+}, and Mn^{4+} peaks are observed in the XPS spectra. (b) La 3d spectrum showing the two spin-orbit peaks, $3d_{5/2}$ and $3d_{3/2}$. Additional peaks due to La bonding with hydroxyl groups and final-state effects are also observed. (c) F 1s spectrum (d) O 1s XPS spectrum with an additional peak at 531.5 eV due to the formation of hydroxyl species.

manganites by divalent atoms (such as in LSMO, LCMO, etc.). It leads to the generation of Mn^{4+} ions at the B (or the Mn) sites of LMOF. With the assumption that the La-deficient sites (we deduce La deficiency of 0.07 per unit cell from EDX measurements) are occupied by Mn^{2+}, we obtain a doping level of 0.07 Mn^{2+} ions per unit cell at the A site. In analogy with A-site doped manganites (with divalent atoms such as Sr, Ca, etc.), we obtain a carrier concentration of 0.07 holes per unit cell. Furthermore, Hall measurement at 300 K confirms hole-type carriers with a concentration of 0.18×10^{22} cm^{-3}. Using the volume of the unit cell obtained from XRD data, we determine the carrier concentration to be 0.11 holes per unit cell, which is comparable with the EDX result. This result further supports Mn^{2+} occupancy of the A sites.

The presence of Mn^{3+} and Mn^{4+} in LMOF does provide a fertile ground for the existence of double exchange, which would explain its metallic and ferromagnetic properties below T_{C1}. On the other hand, F^- doping at the O^{2-} sites will break the Mn^{3+}-O-Mn^{4+} DE chain, which should degrade the metallic and ferromagnetic properties. The Mn ions occupying the A sites have a considerably longer Mn-O bond lengths (2.7 Å) as compared with when the Mn ions occupy the B sites (1.9 Å) [28]. Additionally, the occupation of the La sites by the smaller Mn^{2+} ions would result in lattice distortions which would also lead to a decrease in DE hopping. Against this conflicting backdrop, the observed persisting ferromagnetism and metallic behavior of LMOF is very much intriguing.

A fascinating feature of the LMOF-S2 sample is the presence of two resistivity peaks in $\rho(T)$ data at T_{p1} and T_{p2}. Double peak in the resistivity of manganites have been reported earlier. Such double peaks were ascribed to the presence of excess oxygen in the manganites samples [29], grain size [30], and grain-boundary effects [31,32]. The results of EDX and iodometric titration show oxygen excess in both undoped and F-doped LMO samples. However, double peaks in $\rho(T)$ is observed only in F-doped LMO. This confirms that the double peak feature originates exclusively from F doping. The peak at T_{p2} that originate due to small polycrystal grain size exhibit low MR which is typically less than 20% as reported in the literature [30]. However, the MR at T_{p2} (at 7 T) is high in the LMOF-S2 sample, with a value of 50%. The grain-boundary effects manifest themselves as a gradual increase in MR as the temperature is lowered, with MR increasing to a value which is comparable to the MR value at T_{p1} at the lowest temperatures [33]. No such MR behavior is observed in the LMOF-S2 sample [please see Fig. 6(a)]. The MR is more or less independent of temperature below T_{p2}. The last two observations discount the possibility of grain-size and grain-boundary effects as the origin of double peak in the resistivity data. Another important feature to note is the presence of an additional magnetic transition in the $M(T)$ data at T_{C2}, which roughly corresponds to the second resistivity peak at T_{p2} [see Fig. 6(b)]. Moreover, a large MR of -50% is observed at T_{p2}. These results indicate that the second resistivity peak is related to ferromagnetic properties of the sample.

The persistent ferromagnetism and metallic properties of LMOF may have its origin in the presence of Mn^{2+} ions at the La site. Such occupancy of the A site by divalent Mn^{2+} would explain the hole-type carriers and the
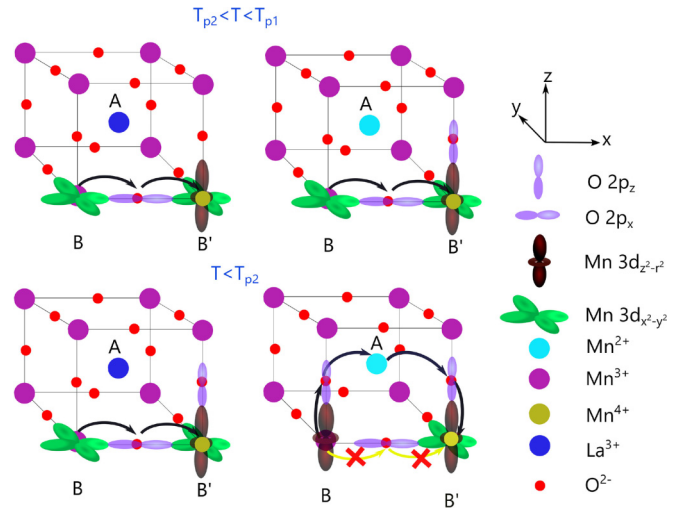

FIG. 8. Schematic of the two DE hopping paths in LMOF. Top panel represents DE hopping in the temperature range $T_{p2} < T < T_{p1}$. The figure on the left shows a lattice with La^{3+} at the A site, whereas on the right we have a lattice with Mn^{2+} at the A site. Hopping takes place by conventional DE along the low resistance path B-B′ for both lattices. The bottom panel depicts the hopping mechanism in the temperature range $T < T_{p2}$. At T_{p2}, local orbital ordering of Mn^{3+} e_g (along the z direction) takes place in the lattice with Mn^{2+} at the A site. As a result orbital overlap takes place along the z direction. Consequently, DE hopping takes place along the high resistance path B-A-B′. In this lattice, conventional DE hopping along B-B′ is forbidden due to lack of orbital overlap along the x direction. On the contrary, for lattice with La^{3+} at the A site, there is no orbital ordering and hence conventional DE hopping along B-B′ survives.

mixed-valent Mn^{3+} and Mn^{4+} ions (in the LMOF sample) observed in the Hall and XPS measurements, respectively. The observed ferromagnetism may also originate from excess oxygen in LMOF. The excess oxygen can increase Mn^{4+} concentration thereby facilitating double exchange. However, we do not observe ferromagnetism and metallic behavior in the undoped LMO sample with a similar oxygen excess. Thus, ferromagnetism in LMOF originates exclusively from F doping. In LMO containing Mn^{2+}, it has been shown that an additional double exchange hopping path via an intermediate Mn^{2+} ion (Mn^{3+}-O-Mn^{2+}-O-Mn^{4+}) exists [28], other than the conventional Mn^{3+} to Mn^{4+} (Mn^{3+}-O-Mn^{4+}) hopping path. This DE hopping path involves electron hopping along B-A-B′ sites (B′ is a neighboring B site) in contrast to conventional DE, where the hopping sites are B-B′ in the manganite lattice (shown in Fig. 8). We suspect that the second peak in the resistivity data at T_{p2} is on account of double exchange hopping along this additional path. The FM ordering at T_{C2}, further lends some credibility to our assumption. We could model the LMOF sample as consisting of some Mn-ions at B sites (Mn^{3+} and Mn^{4+}) and some at A sites (Mn^{2+}), which exhibit ferromagnetic ordering at different temperatures T_{C1} and T_{C2}, respectively. The ferromagnetic ordering of the A and B sites originate from DE hopping of electrons via the B-B′ and B-A-B′ hopping paths. Furthermore, the two DE paths exhibit different resistance. The higher resistance path

include DE hopping via the Mn^{2+} ions located at the A sites. Due to the decreased angle ($<180°$) between the Mn ions and the longer hopping path, it will have a higher resistance. Whereas the lower resistance path involves DE hopping via the conventional Mn^{3+}-O-Mn^{4+} chains which occupy the B sites with angle between the neighboring Mn ions close to $180°$. In the temperature range of $T_{p2} < T < T_{p1}$ the metallic behavior is due to DE hopping via the low resistance path. At T_{p2} the Mn^{2+} ions at the A sites start to exhibit ferromagnetic order, which implies that a DE hopping via the high resistance path is also activated. One possible trigger for the activation of DE hopping along B-A-B′ is local orbital ordering of Mn^{3+} e_g orbitals. Local ordering of Mn^{3+} e_g orbitals have been observed in thin films of LSMO and LMO [34,35]. Here due to the presence of Mn^{2+} at the A sites, e_g orbitals of Mn^{3+} (at the B sites) order along the z direction (i.e., electrons occupy the $d_{z^2-r^2}$ orbital) [34,35]. Consequently, for those lattices where Mn^{2+} ions occupy the A site, hopping takes place via the $d_{z^2-r^2}$ orbital. It is also interesting to note that this orbital ordering prevailed despite the presence of a tensile strain from the substrate on the LSMO film which would have otherwise preferred an in-plane (i.e., $d_{x^2-y^2}$) orbital ordering [35]. Thus, such local orbital ordering of Mn^{3+} is attributed to the presence of Mn^{2+} at the A-sites. Such a local orbital ordering of Mn^{3+} e_g orbitals is the only possible scenario that favor hopping along B-A-B′ as shown in Fig. 8 (since DE hopping takes place only in the presence of orbital overlap between the participating Mn ions and the intermediate O ion). Mn^{3+} being Jahn-Teller (JT) active, its e_g orbitals ($d_{x^2-y^2}$ and $d_{z^2-r^2}$) are nondegenerate, whereas Mn^{2+} and Mn^{4+} are JT inactive and hence their e_g orbitals are degenerate. In the temperature range $T_{p2} < T < T_{p1}$, electrons occupy the lower energy $d_{x^2-y^2}$ in-plane orbital. As a result the orbital overlap is in the in-plane direction leading to conventional DE (as shown in top panel of Fig. 8). At T_{p2} the Mn^{3+} e_g orbitals in the lattice containing Mn^{2+} ions at the A sites order locally along the out-of plane direction, i.e., the energy of the $d_{z^2-r^2}$ orbital is lowered. Consequently, orbital overlap with the O ions take place along the out-of plane direction as shown in the bottom panel of Fig. 8. This results in a DE hopping along the high resistance B-A-B′ path. Thus, below T_{p2} the electron hopping is along the low resistance B-B′ and high resistance B-A-B′ paths in series. Such low resistance and high resistance paths in series leads to a re-emergent MIT in manganites [36]. The second resistivity upturn at T_{p2} in the LMOF sample can be explained in terms of addition of the resistance of the two paths. Initially at T_{p2}, the resistivity of the sample increases due to the inclusion of the high resistance B-A-B′ path. Below T_{p2}, more number of hopping paths via Mn^{2+} are activated. As a result, the resistance starts to decrease again after an initial increase at T_{p2} as temperature is further lowered.

IV. CONCLUSION

To conclude, we prepared fluorine-doped $LaMnO_3$ polycrystalline samples using the solid-state reaction method. The LMOF samples exhibit ferromagnetic and metallic properties which are similar to La-site-doped manganites. The Curie temperature is 239 K and a high MR of -64% is observed. The ferromagnetic and metallic behavior is ascribed to the DE mechanism. Furthermore, the resistivity data exhibit two resistivity peaks around the same temperature at which the $M(T)$ data exhibit two magnetic transitions. Our XPS studies show the presence of Mn^{2+}, Mn^{3+}, and Mn^{4+} ions in the LMOF-S2 sample. The two peaks in the resistivity data are attributed to the presence of multiple DE hopping paths i.e., one along Mn^{3+}-O-Mn^{4+} and another along Mn^{3+}-O-Mn^{2+}-O-Mn^{4+}. Our study shows that anion site doping of perovskite manganite can be a robust technique to explore new and exciting physics in perovskite manganites.

[1] E. Dagotto, J. Fernandez-Baca, G. Alvarez, S. L. Cooper, A. L. Cornelius, and A. Feiguin, *Nanoscale Phase Separation and Colossal Magnetoresistance: The Physics of Manganites and Related Compounds*, Springer Series in Solid-State Sciences (Springer, Berlin, 2003).

[2] P. Schiffer, A. P. Ramirez, W. Bao, and S.-W. Cheong, Phys. Rev. Lett. **75**, 3336 (1995).

[3] A. I. Tovstolytkin, A. M. Pogorily, D. I. Podyalovskii, V. M. Kalita, A. F. Lozenko, P. O. Trotsenko, S. M. Ryabchenko, A. G. Belous, O. I. V'yunov, and O. Z. Yanchevskii, J. Appl. Phys. **102**, 063902 (2007).

[4] J. Fontcuberta, B. Martinez, A. Seffar, S. Pinol, J. L. Garcia-Munoz, and X. Obradors, Phys. Rev. Lett. **76**, 1122 (1996).

[5] Y. Kalyana Lakshmi, G. Venkataiah, M. Vithal, and P. Venugopal Reddy, Phys. B (Amsterdam, Neth.) **403**, 3059 (2008).

[6] G. J. Snyder, R. Hiskes, S. DiCarolis, M. R. Beasley, and T. H. Geballe, Phys. Rev. B **53**, 14434 (1996).

[7] R. Mahendiran, S. K. Tiwary, A. K. Raychaudhuri, T. V. Ramakrishnan, R. Mahesh, N. Rangavittal, and C. N. R. Rao, Phys. Rev. B **53**, 3348 (1996).

[8] J. He, M.-X. Chen, X.-Q. Chen, and C. Franchini, Phys. Rev. B **85**, 195135 (2012).

[9] M. B. Salamon and M. Jaime, Rev. Mod. Phys. **73**, 583 (2001).

[10] P. Ghising, B. Samantaray, and Z. Hossain, Phys. Rev. B **101**, 024408 (2020).

[11] P. Ghising and Z. Hossain, Phys. Rev. B **100**, 115119 (2019).

[12] Y. Tokura, A. Urushibara, Y. Moritomo, T. Arima, A. Asamitsu, G. Kido, and N. Furukawa, J. Phys. Soc. Jpn. **63**, 3931 (1994).

[13] A. Urushibara, Y. Moritomo, T. Arima, A. Asamitsu, G. Kido, and Y. Tokura, Phys. Rev. B **51**, 14103 (1995).

[14] R. Kusters, J. Singleton, D. Keen, R. McGreevy, and W. Hayes, Phys. B (Amsterdam, Neth.) **155**, 362 (1989).

[15] S. Roy, Y. Q. Guo, S. Venkatesh, and N. Ali, J. Phys.: Condens. Matter **13**, 9547 (2001).

[16] C. Zener, Phys. Rev. **82**, 403 (1951).

[17] D. Bahadur and R. A. Dunlap, Bull. Mater. Sci. **21**, 393 (1998).

[18] M. A. Nowroozi, K. Wissel, J. Rohrer, A. R. Munnangi, and O. Clemens, Chem. Mater. **29**, 3441 (2017).

[19] K. Wissel, J. Heldt, P. B. Groszewicz, S. Dasgupta, H. Breitzke, M. Donzelli, A. I. Waidha, A. D. Fortes, J. Rohrer, P. R. Slater, G. Buntkowsky, and O. Clemens, Inorg. Chem. (Washington, DC, U. S.) **57**, 6549 (2018).

[20] P. M. M. Thygesen, C. A. Young, E. O. R. Beake, F. D. Romero, L. D. Connor, T. E. Proffen, A. E. Phillips, M. G. Tucker, M. A. Hayward, D. A. Keen, and A. L. Goodwin, Phys. Rev. B **95**, 174107 (2017).

[21] J. T. Mefford, W. G. Hardin, S. Dai, K. P. Johnston, and K. J. Stevenson, Nat. Mater. **13**, 726 (2014).

[22] R. Laiho, K. Lisunov, E. Lähderanta, P. Petrenko, J. Salminen, V. Stamov, Y. Stepanov, and V. Zakhvalinskii, J. Phys. Chem. Solids **64**, 2313 (2003).

[23] P. G. de Gennes, Phys. Rev. **118**, 141 (1960).

[24] Z. Huang, W. Zhou, C. Ouyang, J. Wu, F. Zhang, J. Huang, Y. Gao, and J. Chu, Sci. Rep. **5**, 10899 (2015).

[25] J. Töpfer, A. Feltz, D. Gräf, B. Hackl, L. Raupach, and P. Weissbrodt, Phys. Status Solidi A **134**, 405 (1992).

[26] S. Mickevičius, S. Grebinskij, V. Bondarenka, B. Vengalis, K. Šliužienė, B. Orlowski, V. Osinniy, and W. Drube, J. Alloys Compd. **423**, 107 (2006).

[27] P. Ghising, D. Das, S. Das, and Z. Hossain, J. Phys.: Condens. Matter **30**, 285002 (2018).

[28] P. Orgiani, A. Galdi, C. Aruta, V. Cataudella, G. De Filippis, C. A. Perroni, V. Marigliano Ramaglia, R. Ciancio, N. B. Brookes, M. Moretti Sala, G. Ghiringhelli, and L. Maritato, Phys. Rev. B **82**, 205122 (2010).

[29] P. Mandal and S. Das, Phys. Rev. B **56**, 15073 (1997).

[30] N. Zhang, F. Wang, W. Zhong, and W. Ding, J. Phys.: Condens. Matter **11**, 2625 (1999).

[31] H. Ju and H. Sohn, Solid State Commun. **102**, 463 (1997).

[32] M. K. Verma, N. D. Sharma, S. Sharma, N. Choudhary, and D. Singh, J. Alloys Compd. **814**, 152279 (2020).

[33] J. Yang, B. Zhao, R. Zhang, Y. Ma, Z. Sheng, W. Song, and Y. Sun, Solid State Commun. **132**, 83 (2004).

[34] A. Galdi, C. Aruta, P. Orgiani, N. B. Brookes, G. Ghiringhelli, M. Moretti Sala, R. V. K. Mangalam, W. Prellier, U. Lüders, and L. Maritato, Phys. Rev. B **83**, 064418 (2011).

[35] C. Aruta, M. Minola, A. Galdi, R. Ciancio, A. Y. Petrov, N. B. Brookes, G. Ghiringhelli, L. Maritato, and P. Orgiani, Phys. Rev. B **86**, 115132 (2012).

[36] T. Z. Ward, S. Liang, K. Fuchigami, L. F. Yin, E. Dagotto, E. W. Plummer, and J. Shen, Phys. Rev. Lett. **100**, 247204 (2008).